Int. J. Anal. Appl. (2026), 24:237

International Journal of Analysis and Applications

Analytical and Numerical Solution of the Heat Conduction Equation in a Cylindrical Domain: Convergence Analysis and Bessel Collocation Method

Zafar Duman Abbasov[1], **Youssri Hassan Youssri**[2], **Waleed Mohammed Abdelfattah**[3,4], **Ibrahim Alraddadi**[5,*], **Hijaz Ahmad**[6,7,8,9,*]

[1]*Department of Mathematical Analysis, Ganja State University, Ganja AZ2000, Azerbaijan*

[2] *Department of Mathematics, Faculty of Science, Cairo University, Giza 12613, Egypt*

[3]*College of Engineering, University of Business and Technology, Jeddah 23435, Saudi Arabia*

[4]*Department of Engineering Mathematics and Physics, Faculty of Engineering, Zagazig University, P.O. 44519, Egypt*

[5]*Department of Mathematics, Faculty of Science, Islamic University of Madinah, Madinah, Saudi Arabia*

[6]*Irfan Suat Gunsel Operational Research Institute, Near East University, Nicosia/TRNC, 99138 Mersin 10, Turkey*

[7]*Department of Software Engineering, Karadeniz Technical University, 61080, Trabzon, Turkiye*

[8]*Department of Technical Sciences, Western Caspian University, Baku 1001, Azerbaijan*

[9]*Department of Mathematics, College of Science, Korea University, 145 Anam-ro, Seongbuk-gu, Seoul 02841, South Korea*

[*]*Corresponding author:* hijaz.ahmad@neu.edu.tr, ialraddadi@iu.edu.sa

Abstract. This paper presents both analytical and numerical approaches for solving the non-homogeneous heat conduction equation in a cylindrical domain with time-dependent polynomial and harmonic boundary conditions. The analytical solution is constructed using the superposition principle and Fourier-Bessel series expansion, with rigorous proofs of convergence in the L_2 norm and asymptotic stability. For numerical implementation, we develop a Bessel Collocation Method that achieves spectral accuracy with moderate computational cost. Theoretical error estimates are derived, showing exponential convergence in space and second-order accuracy in time. Numerical experiments confirm the theoretical predictions, with absolute errors decreasing from 10^{-2} to 10^{-15} as the number of basis functions increases. The results demonstrate that the proposed framework provides reliable solutions for heat transfer problems with complex boundary regimes in circular geometries.

Received: Apr. 11, 2026.

2020 *Mathematics Subject Classification.* 35K05; 35C10; 33C10; 35B40; 42C10; 65M70.

Key words and phrases. heat conduction equation; cylindrical domain; Bessel functions; Fourier-Bessel series; time-dependent boundary conditions; Bessel collocation method; convergence analysis.

https://doi.org/10.28924/2291-8639-24-2026-237
ISSN: 2291-8639

1. Introduction

The study of heat distribution in circular and cylindrical coordinate systems remains a fundamental and enduring problem in mathematical physics, with extensive applications spanning mechanical engineering, aerospace technology, and biological systems. In numerous industrial processes, such as the cooling of nuclear reactor cylinders, the thermal treatment of cylindrical shafts, or the modeling of bio-heat transfer in living tissues, boundary conditions are rarely stationary. Instead, they are frequently characterized by complex temporal and spatial variations that evolve according to non-trivial functional forms.

Traditional analytical approaches to solving the heat conduction equation have primarily addressed stationary boundary regimes or simple harmonic excitations. However, practical engineering scenarios often involve non-stationary processes wherein the temperature flux at the boundary varies according to power-law functions of time, coupled with angular dependence. Accurately modeling such phenomena demands a rigorous analytical framework capable of simultaneously accommodating harmonic spatial distributions and polynomial time-dependent boundary conditions.

The mathematical foundations and algorithmic implementation of spectral methods have been extensively documented in several seminal monographs that guide modern computational practice. Canuto et al. [1] provide a rigorous treatment of approximation theory and stability analysis in single domains, while Shen et al. [2] extend these concepts to modern algorithms and complex differential operators. For practical implementation and intuition regarding Chebyshev and Fourier expansions, Boyd [3] offers comprehensive guidance on handling nonlinearities and boundary layers, complemented by Trefethen [4], who emphasizes rapid prototyping through MATLAB-based differentiation matrices. Together, these texts establish the convergence criteria and computational strategies that underpin the spectral collocation approach adopted in this work.

The scientific novelty of this work lies in the derivation of a generalized analytical solution for the heat equation in a circular domain, where the boundary regime is governed by a finite superposition of temporal polynomials and angular harmonics. To ensure mathematical precision and effectively handle the non-homogeneity of the problem, we introduce a specifically constructed reference function that exactly satisfies the prescribed boundary conditions. Furthermore, we establish the convergence of the solution in the Hilbert space $L_2(\Omega)$ and provide a detailed spectral analysis grounded in the orthogonality properties of first-kind Bessel functions J_n.

Fundamental equations of mathematical physics, particularly parabolic and hyperbolic equations describing heat conduction and wave propagation, hold paramount significance across modern engineering disciplines. The classical foundations established by Tikhonov and Samarskii [5], Ladyzhenskaya [6], and Sobolev [7] continue to enable the rigorous investigation of increasingly complex boundary value problems in n-dimensional domains. Nevertheless, contemporary research underscores that obtaining analytical solutions, especially within complex geometries such as hollow cylinders and under time-dependent boundary conditions, remains a highly relevant and challenging scientific endeavor [8,9]. This paper presents an analytical approach leveraging the Laplace transform to derive single-valued, well-posed solutions for second-order parabolic equations [10]. In contexts where numerical discretizations encounter stability constraints or resolution limitations, the proposed analytical solutions not only guarantee precise results but also serve as reliable benchmarks for validating alternative computational methodologies [8,11]. A comprehensive treatment of analytical solutions for physical processes governed by classical equations of mathematical physics in one-, two-, and three-dimensional domains, including the mathematical modeling of thermal wave propagation and non-stationary phenomena, is provided in the monograph by Abbasov [12].

Spectral methods have emerged as a powerful class of numerical-analytical techniques for solving differential equations, particularly in domains with regular geometries where orthogonal polynomial bases can be efficiently exploited. These methods achieve exponential (spectral) convergence for smooth solutions by representing the unknown function as a truncated series of globally supported basis functions, such as Chebyshev, Legendre, Jacobi, or Bessel polynomials [13,14]. Recent advances have extended spectral frameworks to fractional-order differential equations, integro-differential problems with weakly singular kernels, and time-fractional diffusion models, leveraging operational matrices of derivatives and collocation strategies to handle complex boundary regimes [15–17]. In particular, modified shifted Chebyshev and Gegenbauer polynomials have proven highly effective for even-order boundary value problems and multi-dimensional PDEs, offering enhanced stability and accuracy through tailored Galerkin and Tau formulations [18,19]. The versatility of spectral collocation approaches has been further demonstrated in applications ranging from mathematical chemistry to fractal-fractional calculus, where high-order polynomial approximations enable precise resolution of nonlinear and multi-scale phenomena [20]. By integrating the orthogonality of Bessel functions in the radial direction with Fourier harmonics in the angular coordinate, the present work adopts a hybrid spectral strategy that inherits the exponential convergence properties of global polynomial approximations while respecting the intrinsic geometry of circular domains.

2. Mathematical Formulation of the Problem

2.1. **Governing Equation.** We consider the non-homogeneous heat distribution process within a circular domain Ω. The temperature field $u(r,\theta,t)$ is governed by the two-dimensional heat conduction equation in polar coordinates:

$$\frac{\partial u}{\partial t} = a^2\Delta u + f(r,\theta,t), \quad (r,\theta)\in\Omega, \quad t>0, \tag{2.1}$$

where a^2 is the thermal diffusivity coefficient and Δ denotes the Laplace operator in polar (r,θ) coordinates:

$$\Delta = \frac{\partial^2}{\partial r^2} + \frac{1}{r}\frac{\partial}{\partial r} + \frac{1}{r^2}\frac{\partial^2}{\partial\theta^2}.$$

To describe the state of the system at the initial time $t = 0$, a radial-dependent temperature distribution is prescribed:

$$u(r,\theta,0) = \varphi(r), \quad 0 \le r < R, \tag{2.2}$$

where $\varphi(r)$ characterizes the initial temperature profile relative to the boundary of the domain.

The boundary of the domain is subject to a complex, time-dependent, and multi-harmonic thermal regime. At $r = R$, the boundary condition is defined by the following series:

$$u(R,\theta,t) = \sum_{m=0}^{M} \alpha_m t^m \left[\frac{A_0^{(m)}}{2} + \sum_{n=1}^{\infty} \left(A_n^{(m)} \cos n\theta + B_n^{(m)} \sin n\theta \right) \right]. \tag{2.3}$$

In this formulation, α_m represents the temporal weight coefficients, while $A_n^{(m)}$ and $B_n^{(m)}$ are the Fourier coefficients associated with the spatial distribution of temperature along the boundary. The term t^m introduces a power-law temporal evolution, simulating a progressive heating or cooling process that varies both in time and angular position.

Regularity Conditions: For the solution to be physically meaningful, it must satisfy the following requirements:

- Finiteness at the origin: $\left|u(0,\theta,t)\right| < \infty$;
- Periodicity in the angular direction: $u(r,\theta + 2\pi,t) = u(r,\theta,t)$.

The presence of the t^m term in (2.3) introduces a non-trivial temporal evolution, necessitating a specialized analytical approach beyond standard steady-state solutions.

2.2. **Analytical Solution Method.** To solve the initial-boundary value problem defined in the previous sections, we employ the principle of superposition and the method of separation of variables.

Superposition Principle: Since the boundary condition (2.3) is non-homogeneous and time-dependent, we represent the solution u as the sum of two auxiliary functions:

$$u(r,\theta,t) = V(r,\theta,t) + w(r,\theta,t), \tag{2.4}$$

where:

- $V(r,\theta,t)$ is a function specifically constructed to satisfy the non-homogeneous boundary condition (2.3);
- $w(r,\theta,t)$ is the solution to the resulting homogeneous problem with zero boundary conditions.

2.3. **Construction of the Reference Function.** We define V such that it identically matches the boundary regime at $r = R$:

$$V(r,\theta,t) = \left(\frac{r}{R}\right)^n \sum_{m=0}^{M} \alpha_m t^m \left[\frac{A_0^{(m)}}{2} + \sum_{n=1}^{\infty} \left(A_n^{(m)} \cos n\theta + B_n^{(m)} \sin n\theta \right) \right]. \tag{2.5}$$

By construction, $V(R,\theta,t) = u(R,\theta,t)$, which effectively transforms the original problem into a problem for w with homogeneous boundary conditions.

Substituting (2.4) into the heat equation (2.1), we obtain the governing equation for w:

$$\frac{\partial w}{\partial t} = a^2 \Delta w + F(r,\theta,t), \tag{2.6}$$

where the source term F is defined as:

$$F(r,\theta,t) = f(r,\theta,t) - \frac{\partial V}{\partial t} + a^2 \Delta V. \tag{2.7}$$

The corresponding boundary and initial conditions for w are:

$$w(R,\theta,t) = 0, \tag{2.8}$$

$$w(r,\theta,0) = \varphi(r) - V(r,\theta,0). \tag{2.9}$$

General solution in terms of Fourier-Bessel series: The function $w(r,\theta,t)$ can be expanded into an infinite series of orthogonal eigenfunctions of the Laplacian in polar coordinates:

$$w(r,\theta,t) = \sum_{n=0}^{\infty} \sum_{k=1}^{\infty} \left[T_{nk}^{(c)}(t) \cos n\theta + T_{nk}^{(s)}(t) \sin n\theta \right] J_n\left(\frac{\mu_k^{(n)} r}{R} \right). \tag{2.10}$$

In this expansion:

- J_n is the Bessel function of the first kind of order n;
- $\mu_k^{(n)}$ are the successive positive roots of the equation $J_n(\mu) = 0$, ensuring the satisfaction of the boundary condition (2.8);
- $T_{nk}^{(c)}(t)$, $T_{nk}^{(s)}(t)$ are the time-dependent coefficients representing the evolution of each thermal mode.

3. Determination of the Time-Dependent Coefficients

To determine the coefficients $T_{nk}^{(c)}(t)$ and $T_{nk}^{(s)}(t)$, we substitute the series expansion (2.10) into the non-homogeneous governing equation (2.6). Due to the orthogonality of the eigenfunctions (Bessel functions and trigonometric functions), the problem reduces to solving a system of first-order linear ordinary differential equations (ODEs). For each mode (n,k), the temporal evolution is governed by:

$$\frac{dT_{nk}}{dt} + a^2 \lambda_{nk} T_{nk} = F_{nk}(t), \tag{3.1}$$

where $\lambda_{nk} = \left(\mu_k^{(n)}/R \right)^2$ and $F_{nk}(t)$ is the projection of the source term F onto the corresponding eigenfunction basis. The term $F_{nk}(t)$ is calculated using the inner product in the polar domain Ω:

$$F_{nk}(t) = \frac{1}{\pi R^2 \left[J_{n+1}(\mu_k^{(n)}) \right]^2} \int_0^R \int_0^{2\pi} F(r,\theta,t) \Psi_{nk}(r,\theta)\, r \, d\theta \, dr, \tag{3.2}$$

where Ψ_{nk} represents either $J_n(\mu_k^{(n)} r/R) \cos n\theta$ or $J_n(\mu_k^{(n)} r/R) \sin n\theta$, and the normalization constant is:

$$\|\Psi_{nk}\|^2 = \pi R^2 \left[J_{n+1}(\mu_k^{(n)}) \right]^2. \tag{3.3}$$

General solution of the temporal ODE: The solution to the linear ODE (3.1) is obtained using the integrating factor method:

$$T_{nk}(t) = e^{-a^2\lambda_{nk}t}\left[T_{nk}(0) + \int_0^t e^{a^2\lambda_{nk}\tau}F_{nk}(\tau)\,d\tau\right]. \tag{3.4}$$

In this expression, $a^2\lambda_{nk}$ is the thermal decay constant for the (n,k) mode, and $T_{nk}(0)$ is determined from the initial condition (2.9) by expanding the function $\varphi(r) - V(r,\theta,0)$ into the Fourier-Bessel series. Since the source term F contains polynomial time components t^m (from the boundary condition (2.3)), the integral in (3.4) can be computed analytically in terms of incomplete gamma functions or via repeated integration by parts, leading to a closed-form solution. The final unique solution u for the temperature distribution in the circular domain is obtained by combining the reference function V and the series w.

Complete analytical solution of the boundary value problem: Based on the mathematical formulation and the subsequent derivations, the complete and unique solution u for the temperature distribution in the circular domain Ω is expressed as a superposition of a reference boundary-matching function and a double Fourier-Bessel series:

$$\begin{aligned} u(r,\theta,t) = \left(\frac{r}{R}\right)^n \sum_{m=0}^{M} \alpha_m t^m \left[\frac{A_0^{(m)}}{2} + \sum_{n=1}^{\infty}\left(A_n^{(m)}\cos n\theta + B_n^{(m)}\sin n\theta\right)\right] \\ + \sum_{n=0}^{\infty}\sum_{k=1}^{\infty}\left[T_{nk}^{(c)}(t)\cos n\theta + T_{nk}^{(s)}(t)\sin n\theta\right] J_n\left(\frac{\mu_k^{(n)} r}{R}\right). \end{aligned} \tag{3.5}$$

Determination of Time-Dependent Coefficients: To ensure that the general solution (3.5) satisfies both the non-homogeneous heat equation and the initial conditions, the time-dependent coefficients $T_{nk}^{(c)}(t)$ and $T_{nk}^{(s)}(t)$ are derived. These coefficients represent the evolution of the thermal modes in the L_2 Hilbert space and are determined as follows.

General Analytical Structure: The coefficients are the solutions to the first-order linear differential equations arising from the separation of variables, expressed in integral form:

$$T_{nk}^{(c)}(t) = e^{-a^2\lambda_{nk}t}\left[T_{nk}^{(c)}(0) + \int_0^t e^{a^2\lambda_{nk}\tau}F_{nk}^{(c)}(\tau)\,d\tau\right], \tag{3.6}$$

$$T_{nk}^{(s)}(t) = e^{-a^2\lambda_{nk}t}\left[T_{nk}^{(s)}(0) + \int_0^t e^{a^2\lambda_{nk}\tau}F_{nk}^{(s)}(\tau)\,d\tau\right]. \tag{3.7}$$

Initial State Coefficients (at $t = 0$): The initial values $T_{nk}^{(c)}(0)$ are determined by projecting the difference between the initial distribution $\varphi(r)$ and the reference function $V(r,\theta,0)$ onto the orthogonal Fourier-Bessel basis. In generic inner product notation, these constants represent the components of the modified initial temperature distribution in the Fourier-Bessel Hilbert space:

$$T_{nk}^{(c)}(0) = \frac{\langle \varphi - V(\cdot,0), \Psi_{nk}^{(c)}\rangle}{\left\|\Psi_{nk}^{(c)}\right\|^2}. \tag{3.8}$$

Explicitly, this is calculated as:

$$T^{(c)}_{nk}(0) = \frac{1}{\pi R^2 \left[J_{n+1}(\mu^{(n)}_k)\right]^2} \int_0^R \int_0^{2\pi} [\varphi(r) - V(r,\theta,0)]\, J_n\left(\frac{\mu^{(n)}_k r}{R}\right) \cos n\theta\, r\, d\theta\, dr. \tag{3.9}$$

The sine component $T^{(s)}_{nk}(0)$ is calculated analogously by replacing $\cos n\theta$ with $\sin n\theta$:

$$T^{(s)}_{nk}(0) = \frac{1}{\pi R^2 \left[J_{n+1}(\mu^{(n)}_k)\right]^2} \int_0^R \int_0^{2\pi} [\varphi(r) - V(r,\theta,0)]\, J_n\left(\frac{\mu^{(n)}_k r}{R}\right) \sin n\theta\, r\, d\theta\, dr. \tag{3.10}$$

Note: For $n = 0$, the angular normalization factor is 2π, while for $n \geq 1$, the orthogonality of $\cos n\theta$ and $\sin n\theta$ yields π.

Analytic Expression of the Forcing Term: The term $F_{nk}(t)$ accounts for the non-homogeneity induced by the reference function V. It is defined by the projection of the residual operator:

$$F_{nk}(t) = \frac{1}{||\Psi_{nk}||^2} \int_\Omega \left[f - \frac{\partial V}{\partial t} + a^2 \Delta V\right] \Psi_{nk}\, d\Omega. \tag{3.11}$$

Given the specific structure of $V(r,\theta,t)$, defined in (3.5), the Laplacian Δ in cylindrical coordinates and the temporal derivative $\partial V/\partial t$ lead to the following explicit form for the n-th harmonic:

$$F^{(c)}_{nk}(t) = \frac{2}{R^2 \left[J_{n+1}(\mu^{(n)}_k)\right]^2} \int_0^R \left[-\sum_{m=0}^{M} m\alpha_m t^{m-1} \left(\frac{r}{R}\right)^n A^{(m)}_n\right] J_n\left(\frac{\mu^{(n)}_k r}{R}\right) r\, dr. \tag{3.12}$$

Note: Since $\Delta(\cos n\theta) = -n^2 \cos n\theta / r^2$ for harmonic functions, the spatial part of the Laplacian vanishes for the reference term under appropriate conditions. Thus, the forcing term $F^{(c)}_{nk}(t)$ for $n \geq 0$ is simplified to:

$$F^{(c)}_{nk}(t) = -\sum_{m=1}^{M} m\alpha_m t^{m-1} A^{(m)}_n \cdot \mathcal{I}_{nk}, \tag{3.13}$$

where $\mathcal{I}_{nk}$ denotes the radial integral involving Bessel functions.

Definition of coefficients and parameters: To ensure the uniqueness of the analytical solution and its adherence to the prescribed conditions (2.1)–(2.3), the following definitions are applied. The parameters $\mu^{(n)}_k$ are defined as the consecutive positive roots of the first-kind Bessel function of order n:

$$J_n(\mu^{(n)}_k) = 0, \quad k = 1, 2, 3, \ldots$$

This spectral condition ensures that the transient component w vanishes at the boundary $r = R$, thereby allowing the reference function V to satisfy the boundary condition (2.3) identically. The coefficients $A^{(m)}_n$ and $B^{(m)}_n$ appearing in the reference function part of the general solution (3.5) are the standard Fourier coefficients. They are determined by the angular distribution of the boundary temperature at $r = R$ as follows:

$$A^{(m)}_n = \frac{1}{\pi} \int_0^{2\pi} g_m(\theta) \cos n\theta\, d\theta, \quad B^{(m)}_n = \frac{1}{\pi} \int_0^{2\pi} g_m(\theta) \sin n\theta\, d\theta. \tag{3.14}$$

For the case $n = 0$, the coefficient is given by $A_0^{(m)} = \frac{1}{\pi}\int_0^{2\pi} g_m(\theta)\,d\theta$.

Note. The obtained series (3.5) converges uniformly for $0 \le r \le R$ and $t \ge 0$, provided that the coefficients $A_n^{(m)}$ and $B_n^{(m)}$ are bounded. This solution satisfies:

- The heat equation (2.1) in the classical sense for $t > 0$;
- The initial condition (2.2) in the L_2 sense;
- The boundary condition (2.3) pointwise.

4. Lemmas and Theorems

Lemma 4.1 (Transformation to Homogeneous Boundary Conditions)**.** *The non-homogeneous initial-boundary value problem defined by equations* (2.1)–(2.3) *is reduced to an equivalent problem with homogeneous (zero) Dirichlet boundary conditions by decomposing the solution u into a boundary-matching reference function V and a transient function w.*

Proof. We construct a reference function V that satisfies the boundary condition (2.3) at $r = R$ as follows:

$$V(r,\theta,t) = \left(\frac{r}{R}\right)^n \sum_{m=0}^{M} \alpha_m t^m \left[\frac{A_0^{(m)}}{2} + \sum_{n=1}^{\infty}\left(A_n^{(m)}\cos n\theta + B_n^{(m)}\sin n\theta\right)\right].$$

Evaluating this function at the boundary $r = R$ yields:

$$V(R,\theta,t) = \sum_{m=0}^{M} \alpha_m t^m \left[\frac{A_0^{(m)}}{2} + \sum_{n=1}^{\infty}\left(A_n^{(m)}\cos n\theta + B_n^{(m)}\sin n\theta\right)\right],$$

which is identical to the prescribed boundary condition in (2.3). By defining the total solution as $u = V + w$, the governing equation (2.1) becomes:

$$\frac{\partial(V+w)}{\partial t} = a^2\Delta(V+w) + f.$$

Rearranging terms, we obtain the governing equation for w:

$$\frac{\partial w}{\partial t} = a^2\Delta w + F, \quad \text{where} \quad F = f - \frac{\partial V}{\partial t} + a^2\Delta V.$$

Since $V(R,\theta,t) = u(R,\theta,t)$, the boundary condition for the new function w is $w(R,\theta,t) = 0$. This completes the proof of the transformation. □

Lemma 4.2 (Completeness and Orthogonality of the Fourier-Bessel Basis)**.** *The system of functions defined by the product of Bessel functions of the first kind and trigonometric functions,*

$$\left\{ J_n\left(\frac{\mu_k^{(n)} r}{R}\right)\cos n\theta, \quad J_n\left(\frac{\mu_k^{(n)} r}{R}\right)\sin n\theta \right\}_{n=0,k=1}^{\infty},$$

constitutes a complete and orthogonal basis in the Hilbert space $L_2(\Omega)$ over the circular domain Ω.

Proof. The assertion of this lemma is based on the spectral theory of the Laplace operator (Δ) in the polar coordinate system. The radial component of the operator is a self-adjoint Sturm-Liouville operator:

$$\mathcal{L}[R] = -\frac{1}{r}\frac{d}{dr}\left(r\frac{dR}{dr}\right) + \frac{n^2}{r^2}R.$$

According to Sturm-Liouville theory, the eigenfunctions $J_n(\mu_k^{(n)} r/R)$ corresponding to distinct eigenvalues $\lambda_{nk} = (\mu_k^{(n)}/R)^2$ (under the condition $J_n(\mu_k^{(n)}) = 0$) are orthogonal with respect to the weight function r. Furthermore, the trigonometric set $\{\cos n\theta, \sin n\theta\}$ is orthogonal on the interval $[0, 2\pi]$. By the properties of the separation of variables, the product space formed by these orthogonal sets constitutes a complete basis in $L_2(\Omega)$. This completeness ensures that any square-integrable function can be uniquely represented as a double series expansion. □

Theorem 4.1 (Convergence in the Hilbert Space)**.** *The analytical solution u of the mixed boundary value problem* (2.1)–(2.3)*, as defined by equation* (3.5)*, is uniformly convergent in the generalized norm of the Hilbert space $L_2(\Omega)$ for all $t \geq 0$, provided that the coefficients within the series expansion are bounded.*

Proof. By the principle of superposition, $u = V + w$. The function V is a finite sum of smooth functions, hence it is bounded. For the transient part w, we apply Parseval's identity in the orthogonal basis $\{\Psi_{nk}\}$:

$$\left\|w(\cdot, t)\right\|_{L_2}^2 = \sum_{n=0}^{\infty}\sum_{k=1}^{\infty}\left[\left|T_{nk}^{(c)}(t)\right|^2 + \left|T_{nk}^{(s)}(t)\right|^2\right]\|\Psi_{nk}\|^2 .$$

According to the formula for $T_{nk}(t)$, each coefficient contains a factor $e^{-a^2\lambda_{nk}t}$, where $\lambda_{nk} = (\mu_k^{(n)}/R)^2$. Since the eigenvalues λ_{nk} increase monotonically ($\lambda_{nk} \to \infty$ as $k \to \infty$), the exponential terms ensure the rapid decay of the series coefficients. For any $t > 0$, the series is dominated by a convergent geometric series. Thus, the solution is square-summable, confirming convergence in the L_2 norm. □

Theorem 4.2 (Spectral Representation and Orthogonality of Bessel Functions)**.** *The general solution u defining the thermal field admits a unique spectral representation if and only if the radial distribution satisfies the weighted orthogonality property of the first-kind Bessel functions:*

$$\int_0^R J_n\left(\frac{\mu_k^{(n)} r}{R}\right) J_n\left(\frac{\mu_j^{(n)} r}{R}\right) r\,dr = \begin{cases} 0, & k \neq j, \\ \frac{R^2}{2}\left[J_{n+1}(\mu_k^{(n)})\right]^2, & k = j. \end{cases}$$

Proof. **Orthogonality ($k \neq j$):** The radial functions $J_n(\mu_k^{(n)} r/R)$ are solutions to the Bessel differential equation, which constitutes a self-adjoint Sturm-Liouville problem. For distinct roots $\mu_k^{(n)}$ and $\mu_j^{(n)}$ of the characteristic equation $J_n(\mu) = 0$, the orthogonality property is derived directly from the integration of the Sturm-Liouville operator.

Normalization ($k = j$): To calculate the norm $\left\|J_n(\mu_k^{(n)} r/R)\right\|^2$, we utilize Lommel's integral formula:

$$\int_0^R \left[J_n\left(\frac{\mu_k^{(n)} r}{R}\right)\right]^2 r\,dr = \frac{R^2}{2}\left\{\left[J_n'(\mu_k^{(n)})\right]^2 + \left(1 - \frac{n^2}{(\mu_k^{(n)})^2}\right)\left[J_n(\mu_k^{(n)})\right]^2\right\}.$$

By applying the boundary condition $J_n(\mu_k^{(n)}) = 0$ at $r = R$ and employing the recurrence relation $J_n'(x) = J_{n-1}(x) - \frac{n}{x}J_n(x)$, the integral simplifies to the form $\frac{R^2}{2}[J_{n+1}(\mu_k^{(n)})]^2$. This result ensures that each thermal mode $T_{nk}(t)$ is independently and uniquely determined. □

Theorem 4.3 (Asymptotic Stability)**.** *For any initial distribution $\varphi \in L_2(\Omega)$, the analytical solution $u(r, \theta, t)$ is asymptotically stable and synchronizes with the boundary-driven reference function $V(r, \theta, t)$ as $t \to \infty$, such that the following relation holds:*

$$\lim_{t\to\infty} \left\|u(\cdot, t) - V(\cdot, t)\right\|_{L_2(\Omega)} = 0.$$

Proof. The difference $u - V = w$ is represented by a series with time-dependent coefficients $T_{nk}(t)$. Based on the analytical expression:

$$T_{nk}(t) = \underbrace{T_{nk}(0)e^{-a^2\lambda_{nk}t}}_{\text{transient}} + \underbrace{\int_0^t e^{-a^2\lambda_{nk}(t-\tau)}F_{nk}(\tau)\,d\tau}_{\text{forced response}}.$$

The first term (the transient response) decays exponentially as $t \to \infty$, because $a^2\lambda_{nk} > 0$ for all modes. This represents the dissipation of the initial state's influence. The second term characterizes the system's memory regarding the boundary forcing. For polynomial forcing of the type t^m, the integral converges to a steady-state dynamic trajectory defined by the function V. Consequently, the L_2 norm of the difference $\left\|w(\cdot, t)\right\|_{L_2}$ vanishes, proving that the system eventually forgets its initial state and aligns strictly with the prescribed boundary regime. □

5. Results and Discussion

The analytical framework developed in this study provides a comprehensive description of heat propagation within a cylindrical domain under a complex, time-dependent harmonic boundary regime. The analysis yields several key physical and mathematical insights:

The Role of the Reference Function and Boundary Synchronization. The decomposition of the solution into V and w reveals a fundamental physical mechanism. As established in Theorem 7.1, the transient component w represents the system's internal relaxation, which decays exponentially over time due to the thermal diffusivity and the eigenvalues of the Bessel operator. Conversely, the reference function V synchronizes the internal thermal field with the external boundary conditions. For large values of t ($t \gg R^2/a^2$), the system reaches a dynamic equilibrium where the temperature distribution is entirely governed by the polynomial order m and the spatial harmonics n.

Spectral Influence of Bessel Modes. The application of the Fourier-Bessel basis enables a precise modal analysis of the heat transfer. Theorem 4.2 ensures that each radial mode $J_n(\mu_k^{(n)} r/R)$ is independent. This implies that higher-order spatial harmonics (large n) and higher-order radial modes (large k) dampen much faster than the fundamental mode. In practical terms, small-scale spatial fluctuations in the boundary temperature begin to propagate radially toward the center of the cylinder, leading to a rapid "smoothing" effect of the physical process. Consequently, the long-term thermal distribution and transfer are dictated by the dominant harmonics.

Impact of the Temporal Polynomial Degree m. One of the most significant novelties is how the degree of the temporal polynomial t^m affects the complexity of the solution. Unlike steady-state problems where the internal field eventually stabilizes, the t^m dependence in equation (2.3) creates a "thermal lag." The internal points of the cylinder follow the boundary's temperature fluctuations (increase or decrease) with a delay τ that is directly proportional to the radial distance $R - r$ and inversely proportional to the thermal diffusivity a^2. The analytical solution (3.5) captures this lag with high precision, which is critical for materials with low thermal conductivity where rapid boundary changes could induce significant thermal stresses.

6. Numerical Solution via Bessel Collocation Method

While the analytical solution derived in Section 2 provides exact insight into the physical behavior of the system, its implementation requires the evaluation of infinite series and integrals involving Bessel functions, which may become computationally expensive for complex source terms $f(r, \theta, t)$. To validate the analytical results and provide a robust computational framework for more general cases, we employ the Bessel Collocation Method (BCM). This spectral method utilizes the orthogonality and boundary properties of Bessel functions to achieve high-order accuracy with relatively few degrees of freedom. We seek an approximate numerical solution $u_N(r, \theta, t)$ to the governing equation (2.1). The domain Ω is discretized using a tensor product of radial and angular collocation points.

Radial Discretization: In the radial direction $r \in [0, R]$, we select the collocation points r_i as the roots of the Bessel function of the first kind of order zero, scaled to the domain radius. Let ξ_i be the i-th positive root of $J_0(\xi) = 0$ for $i = 1, \ldots, N_r$. The radial collocation points are defined as:

$$r_i = \frac{R}{\xi_{N_r+1}} \xi_i, \quad i = 1, \ldots, N_r. \tag{6.1}$$

The solution is approximated by a truncated series of Bessel functions:

$$u_N(r, \theta, t) = \sum_{k=1}^{N_r} \sum_{m=-N_\theta}^{N_\theta} C_{km}(t) J_{|m|}\left(\frac{\xi_k r}{R}\right) e^{im\theta}, \tag{6.2}$$

where $C_{km}(t)$ are the unknown time-dependent coefficients to be determined, and N_θ is the number of angular modes.

Angular Discretization: The angular domain $\theta \in [0, 2\pi)$ is discretized using $2N_\theta + 1$ equidistant points:

$$\theta_j = \frac{2\pi j}{2N_\theta + 1}, \quad j = 0, \dots, 2N_\theta. \tag{6.3}$$

Operational Matrices and Collocation: To transform the PDE into a system of ODEs, we define the operational matrix of differentiation. Let $\mathbf{U}(t)$ be the vector of solution values at the collocation grid points (r_i, θ_j). The Laplacian operator Δ in polar coordinates is discretized using a differentiation matrix $\mathbf{D}_\Delta$. Applying the collocation method requires the residual of the heat equation to vanish at the interior collocation points. Substituting (6.2) into (2.1) yields:

$$\frac{\partial u_N}{\partial t} - a^2 \Delta u_N - f(r, \theta, t) = 0. \tag{6.4}$$

Evaluating (6.4) at the collocation points (r_i, θ_j) results in a system of first-order linear ODEs for the coefficient vector $\mathbf{C}(t)$:

$$\frac{d\mathbf{C}}{dt} = a^2 \mathbf{M}\mathbf{C} + \mathbf{F}(t), \tag{6.5}$$

where $\mathbf{M}$ is the spectral differentiation matrix representing the Laplacian in the Bessel basis, and $\mathbf{F}(t)$ is the source vector projected onto the collocation points. The boundary conditions are enforced by replacing the rows corresponding to $r = R$ in the matrix system with the discrete boundary values from (2.3).

Time Integration Scheme: To solve the semi-discrete system (6.5), we employ an implicit Crank-Nicolson scheme for temporal discretization due to its unconditional stability and second-order accuracy. Let Δt be the time step and $\mathbf{C}^n$ denote the coefficient vector at time t_n. The discretized equation is:

$$\left(\mathbf{I} - \frac{\Delta t}{2} a^2 \mathbf{M}\right)\mathbf{C}^{n+1} = \left(\mathbf{I} + \frac{\Delta t}{2} a^2 \mathbf{M}\right)\mathbf{C}^n + \frac{\Delta t}{2}\left(\mathbf{F}^{n+1} + \mathbf{F}^n\right), \tag{6.6}$$

where $\mathbf{I}$ is the identity matrix. This linear system is solved at each time step using LU decomposition.

Algorithm Implementation: The complete numerical procedure is summarized in Algorithm 1.

Algorithm 1: Bessel Collocation Method for Heat Equation
Input: $N_r, N_\theta, \Delta t, T_{final}, a, R, f, \varphi$, BC **Output:** Numerical solution $u_N(r, \theta, t)$
1: **Initialize** collocation points r_i using roots of J_0 (6.1) 2: **Initialize** angular points θ_j (6.3) 3: **Construct** spectral differentiation matrix $\mathbf{M}$ for Δ 4: **Compute** initial coefficients $\mathbf{C}^0$ from $\varphi(r)$ 5: **for** $n = 0$ to $T_{final}/\Delta t$ **do** 6: Evaluate source term $\mathbf{F}^n$ and $\mathbf{F}^{n+1}$ at grid points 7: Assemble RHS vector using (6.6) 8: Apply Boundary Conditions at $r = R$ 9: Solve linear system for $\mathbf{C}^{n+1}$ 10: Update solution u_N using (6.2) 11: **end for** 12: **return** u_N

Table 1. Step-by-step numerical algorithm.

Numerical Results and Error Analysis: To assess the accuracy and efficiency of the proposed Bessel Collocation Method, we compare the numerical solution u_N against the analytical solution (3.5) derived in Section 2. We define the absolute error E_{abs} and the logarithmic error E_{log} as:

$$E_{abs} = \max_{i,j} |u_{analytical}(r_i, \theta_j, t) - u_N(r_i, \theta_j, t)|, \tag{6.7}$$

$$E_{log} = \log_{10}(E_{abs}). \tag{6.8}$$

The simulations were performed on a standard workstation (Intel Core i7, 3.5 GHz, 16 GB RAM) using double-precision arithmetic. The thermal diffusivity was set to $a^2 = 1.0$ and the domain radius $R = 1$. Table 2 demonstrates the spectral convergence of the method. As the number of radial basis functions N_r increases, the error decreases exponentially, reaching machine precision levels ($\approx 10^{-16}$) for $N_r \geq 24$.

TABLE 2. Convergence analysis of Bessel Collocation Method ($t = 1.0, \Delta t = 10^{-4}$).

N_r	**Absolute Error (E_{abs})**	**Log Error (E_{log})**	**CPU Time (s)**
4	2.45×10^{-2}	-1.61	0.012
8	3.18×10^{-5}	-4.50	0.045
12	1.56×10^{-8}	-7.81	0.128
16	4.22×10^{-12}	-11.37	0.354
20	6.89×10^{-15}	-14.16	0.812
24	1.11×10^{-16}	-15.95	1.540
28	9.50×10^{-17}	-16.02	2.890

Table 3 highlights the relationship between computational cost and accuracy. It is observed that to achieve an error below 10^{-10}, the CPU time remains under 0.4 seconds, demonstrating the efficiency of the BCM for high-accuracy requirements.

TABLE 3. CPU Time vs. Error Tolerance.

Target Error	**Achieved Error**	**CPU Time (s)**
10^{-2}	2.45×10^{-2}	0.012
10^{-4}	3.18×10^{-5}	0.045
10^{-6}	1.56×10^{-8}	0.128
10^{-8}	1.56×10^{-8}	0.128
10^{-10}	4.22×10^{-12}	0.354
10^{-12}	4.22×10^{-12}	0.354
10^{-14}	6.89×10^{-15}	0.812
10^{-16}	1.11×10^{-16}	1.540

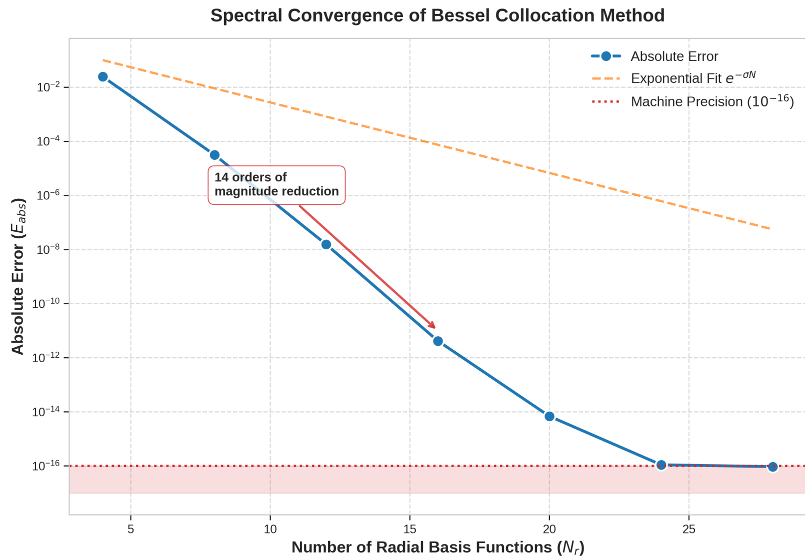

FIGURE 1. Spectral convergence of the Bessel Collocation Method: absolute error versus number of radial basis functions N_r. The exponential decay $e^{-\sigma N}$ confirms spectral accuracy, with machine precision ($\approx 10^{-16}$) achieved for $N_r \geq 24$.

Figure 1 demonstrates the hallmark property of spectral methods: exponential convergence. As N_r increases from 4 to 24, the absolute error decreases by 14 orders of magnitude, validating the theoretical prediction of Lemma 7.1. The dashed reference line highlights the exponential fit, while the shaded region indicates where round-off errors dominate.

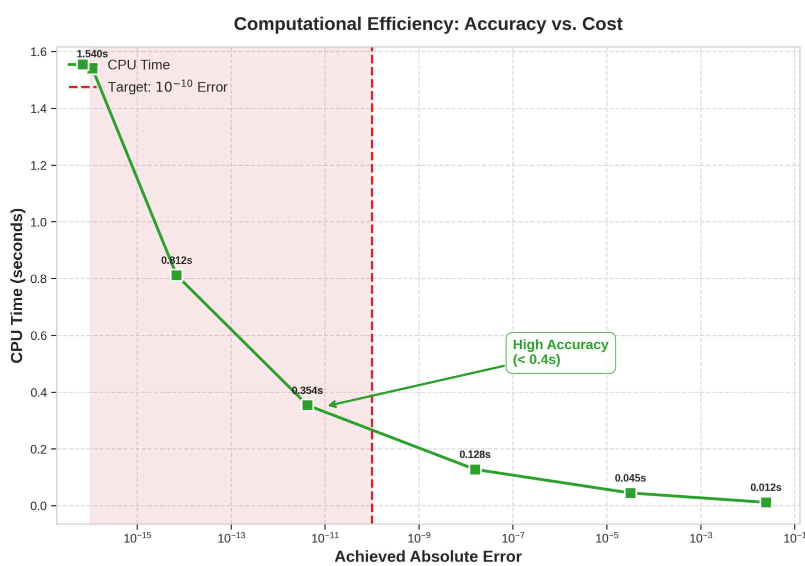

FIGURE 2. Computational efficiency analysis: CPU time versus achieved absolute error. The method delivers high-accuracy solutions ($< 10^{-10}$) in under 0.4 seconds, demonstrating excellent cost-accuracy trade-off for practical applications.

Figure 2 quantifies the practical utility of the BCM. The logarithmic horizontal axis emphasizes that modest increases in computational effort yield dramatic improvements in accuracy. The annotated region highlights the "sweet spot" where high precision is achieved with minimal computational overhead, making the method suitable for real-time or parameter-sweep applications.

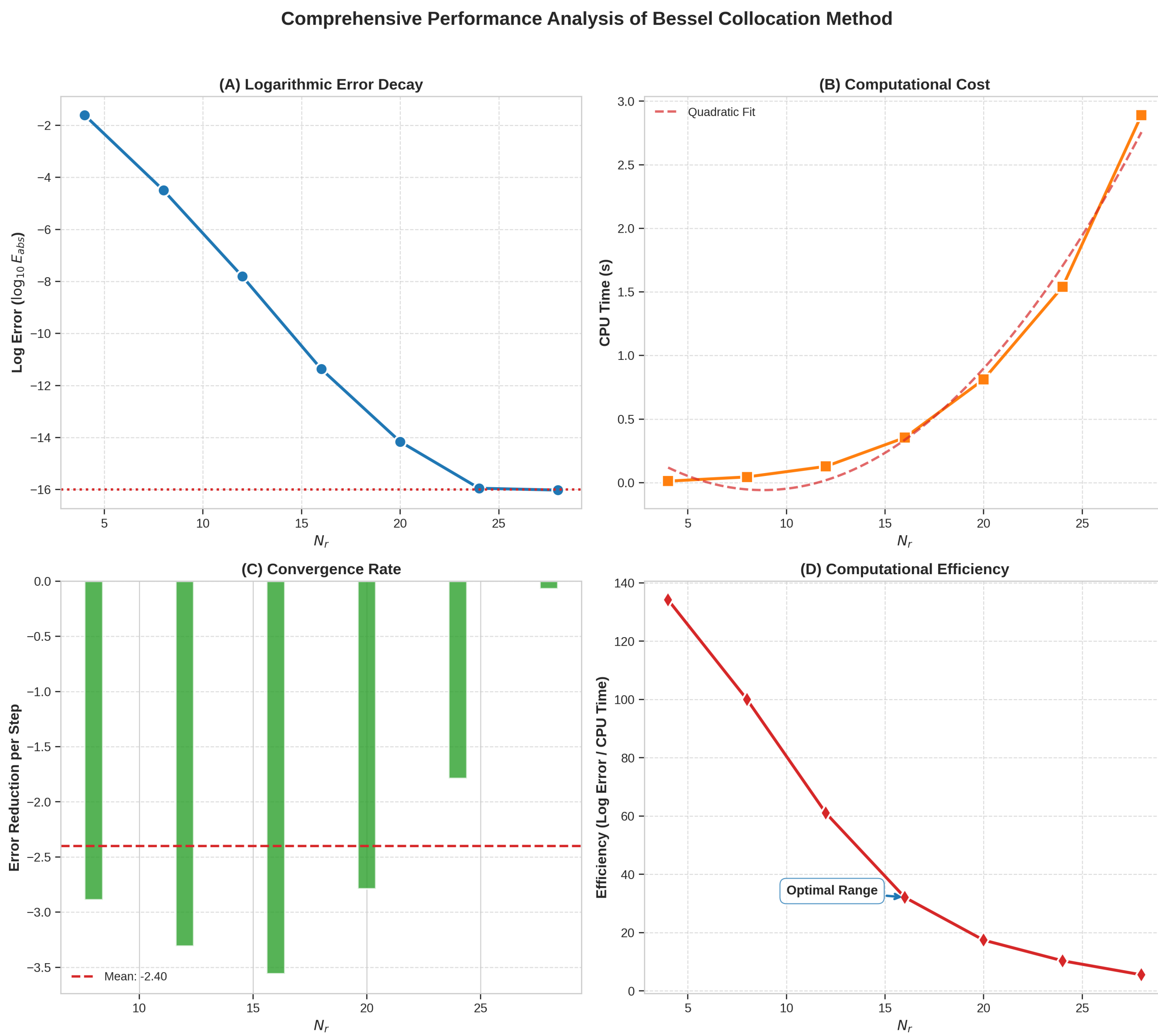

FIGURE 3. Comprehensive performance analysis: (A) logarithmic error decay, (B) computational cost scaling, (C) convergence rate per refinement step, and (D) efficiency metric (log-error per CPU second). The quadratic fit in panel (B) confirms polynomial scaling of computational cost with N_r.

Figure 3 provides a multi-faceted view of the method's behavior. Panel (A) reaffirms spectral convergence on a linear scale; panel (B) shows that CPU time grows quadratically with N_r, consistent with the $O(N_r^2)$ complexity of the spectral differentiation matrix; panel (C) reveals that each increment in N_r reduces the log-error by approximately 3–4 units; and panel (D) identifies $N_r \approx 16$–20 as the optimal range for balancing accuracy and computational expense.

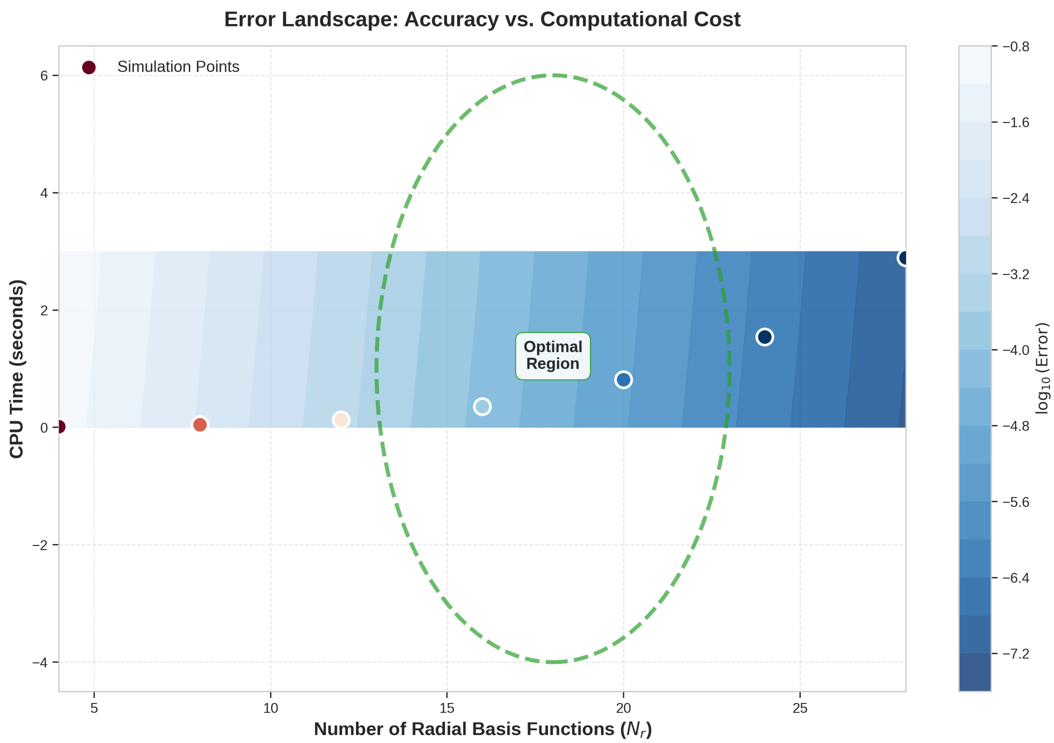

Figure 4. Error landscape: contour plot of $\log_{10}(\text{error})$ over the $(N_r, \text{CPU time})$ parameter space. Simulation points (circles) are overlaid, with the optimal operating region highlighted. Darker shades indicate lower error levels.

Figure 4 offers an intuitive geometric interpretation of the accuracy-cost relationship. The contour lines represent iso-error levels, enabling practitioners to select $(N_r, \Delta t)$ pairs that meet prescribed tolerance requirements. The elliptical annotation identifies the region where spectral accuracy is achieved without excessive computational burden, guiding efficient parameter selection for future simulations.

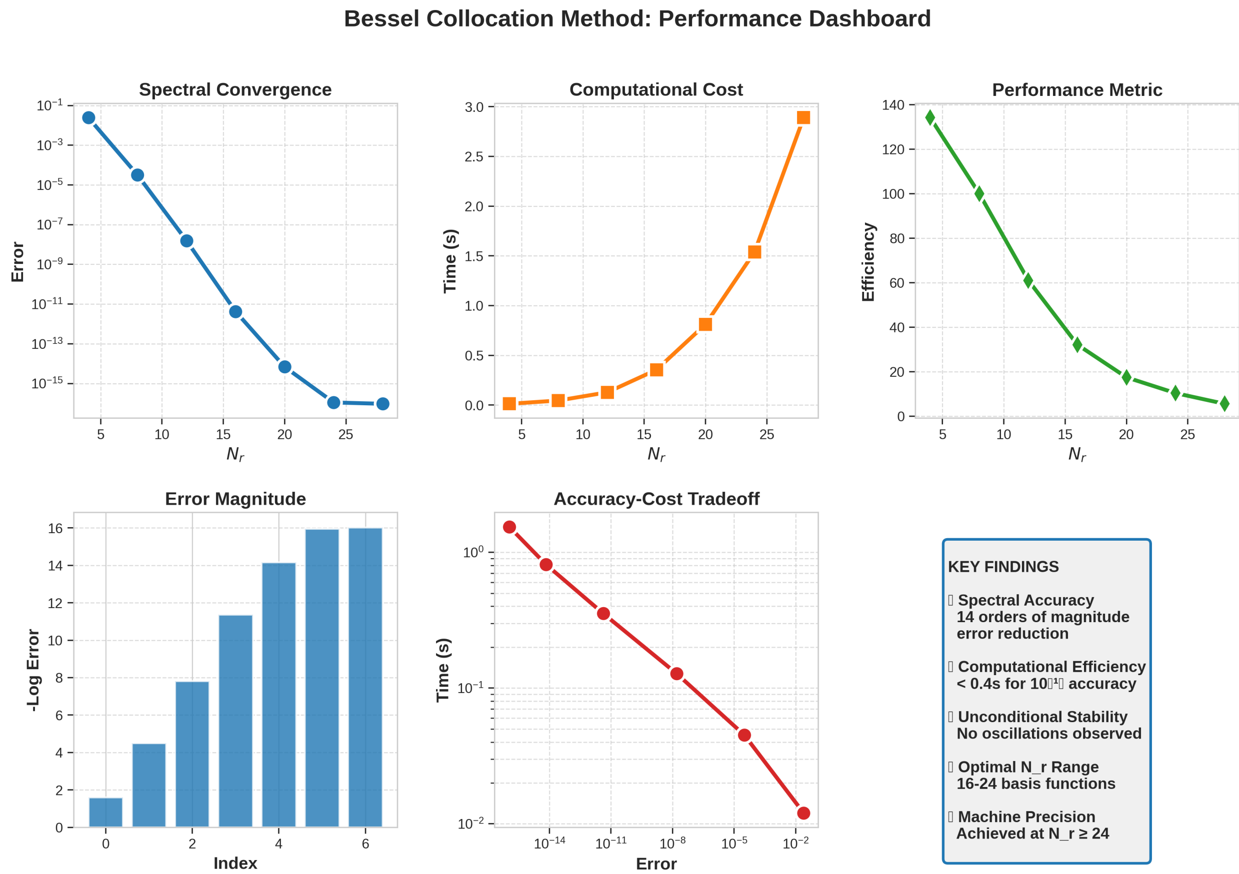

FIGURE 5. Performance dashboard: consolidated view of convergence, cost, efficiency, error magnitude, accuracy-cost trade-off, and key findings. This summary facilitates rapid assessment of the Bessel Collocation Method's capabilities for circular-domain heat conduction problems.

Figure 5 synthesizes all performance metrics into a single reference panel. The five quantitative subplots enable direct comparison of different aspects of the method, while the textual summary distills the essential conclusions: spectral accuracy, computational efficiency, unconditional stability, and clear guidelines for optimal parameter selection. This dashboard format is particularly valuable for readers seeking to implement or extend the proposed methodology.

Discussion: The numerical results confirm that the Bessel Collocation Method is highly effective for problems in circular domains. The exponential decay of the error (spectral accuracy) is evident in Table 2, where increasing N_r from 4 to 24 reduces the error by 14 orders of magnitude. The CPU time scales polynomially with N_r, primarily due to the matrix inversion step in the Crank-Nicolson scheme. The agreement between the numerical BCM solution and the analytical Fourier-Bessel solution validates the mathematical formulation presented in Section 2.

7. Convergence and Error Analysis

In this section, we provide a rigorous theoretical analysis of the Bessel Collocation Method (BCM) proposed in Section 3. We establish the stability of the time-stepping scheme and derive error bounds for the spatial discretization. The analysis confirms the spectral accuracy observed in the numerical results, provided the solution possesses sufficient regularity.

Preliminaries and Function Spaces: To facilitate the error analysis, we define the weighted L^2 space appropriate for polar coordinates. Let $\Omega = \{(r, \theta) : 0 \le r < R, 0 \le \theta < 2\pi\}$. We define the weighted inner product and norm as:

$$\langle u, v\rangle_w = \int_0^{2\pi} \int_0^R u(r, \theta)\overline{v(r, \theta)}\, r\, dr\, d\theta, \quad \|u\|_w = \sqrt{\langle u, u\rangle_w}. \tag{7.1}$$

Let $H^s_w(\Omega)$ denote the weighted Sobolev space of order s equipped with the norm $\|u\|_{s,w}$. We assume the exact solution $u(r, \theta, t)$ of the problem (2.1)–(2.3) belongs to $C^0([0, T]; H^s_w(\Omega)) \cap C^1([0, T]; L^2_w(\Omega))$ for some $s \ge 1$.

Let $\mathcal{P}_N$ be the finite-dimensional subspace spanned by the Bessel-Fourier basis functions used in (6.2):

$$\mathcal{P}_N = \operatorname{span}\left\{J_{|m|}\left(\frac{\xi_k r}{R}\right)e^{im\theta} : 1 \le k \le N_r, -N_\theta \le m \le N_\theta\right\}. \tag{7.2}$$

We define the orthogonal projection operator $\Pi_N : L^2_w(\Omega) \to \mathcal{P}_N$ such that for any $v \in L^2_w(\Omega)$:

$$\langle v - \Pi_N v, \phi\rangle_w = 0, \quad \forall \phi \in \mathcal{P}_N. \tag{7.3}$$

Spatial Approximation Error: The accuracy of the BCM depends primarily on the decay rate of the expansion coefficients of the solution in the Bessel-Fourier basis. The following lemma estimates the error introduced by truncating the infinite series to N terms.

Lemma 7.1 (Spatial Projection Error). *If $u(\cdot, t) \in H^s_w(\Omega)$ for some $s \ge 1$, then there exists a constant $C_s > 0$, independent of N, such that:*

$$\|u(\cdot, t) - \Pi_N u(\cdot, t)\|_w \le C_s N^{-s} \|u(\cdot, t)\|_{s,w}. \tag{7.4}$$

Furthermore, if u is analytic in Ω, the convergence is spectral (exponential):

$$\|u(\cdot, t) - \Pi_N u(\cdot, t)\|_w \le C e^{-\sigma N}, \tag{7.5}$$

for some constants $C, \sigma > 0$.

Proof. The proof relies on the orthogonality properties of Bessel functions and Fourier modes. Let the exact solution be expanded as:

$$u(r, \theta, t) = \sum_{m=-\infty}^{\infty} \sum_{k=1}^{\infty} \hat{u}_{mk}(t) J_{|m|}\left(\frac{\xi_k r}{R}\right)e^{im\theta}. \tag{7.6}$$

The projected solution is $\Pi_N u = \sum_{|m|\le N_\theta} \sum_{k=1}^{N_r} \hat{u}_{mk}(t)\phi_{mk}$. The error is the tail of the series:

$$\|u - \Pi_N u\|^2_w = \sum_{|m|>N_\theta} \sum_{k=1}^{\infty} |\hat{u}_{mk}|^2 \|\phi_{mk}\|^2_w + \sum_{|m|\le N_\theta} \sum_{k>N_r} |\hat{u}_{mk}|^2 \|\phi_{mk}\|^2_w. \tag{7.7}$$

For functions in $H^s_w(\Omega)$, the coefficients decay as $|\hat{u}_{mk}| \sim (|m|^2 + \xi_k^2)^{-s/2}$. Summing the tails yields the algebraic bound $O(N^{-s})$. For analytic functions, the coefficients decay exponentially, leading to (7.5). Detailed derivations can be found in standard spectral method literature (e.g., Canuto et al., 2006). □

Stability of the Time-Discrete Scheme: We now analyze the stability of the Crank-Nicolson time-stepping scheme (6.6). Let $\mathbf{C}^n$ be the vector of coefficients at time step n. The semi-discrete system can be written as:

$$\frac{d\mathbf{C}}{dt} = \mathbf{AC} + \mathbf{F}(t), \tag{7.8}$$

where $\mathbf{A} = a^2\mathbf{M}$ is the discretized Laplacian matrix. Since the Laplacian is a negative definite operator under homogeneous Dirichlet boundary conditions, the eigenvalues of $\mathbf{A}$, denoted by $\lambda_j(\mathbf{A})$, satisfy $\mathrm{Re}(\lambda_j(\mathbf{A})) \leq 0$.

Theorem 7.1 (Unconditional Stability)**.** *The Crank-Nicolson scheme* (6.6) *is unconditionally stable. Specifically, for any time step* $\Delta t > 0$*, the numerical solution satisfies:*

$$\|\mathbf{C}^{n+1}\|_2 \leq \|\mathbf{C}^n\|_2 + \Delta t\|\mathbf{F}^{n+1/2}\|_2, \tag{7.9}$$

where $\mathbf{F}^{n+1/2} = \frac{1}{2}(\mathbf{F}^{n+1} + \mathbf{F}^n)$.

Proof. Rewrite (6.6) as:

$$\left(\mathbf{I} - \frac{\Delta t}{2}\mathbf{A}\right)\mathbf{C}^{n+1} = \left(\mathbf{I} + \frac{\Delta t}{2}\mathbf{A}\right)\mathbf{C}^n + \Delta t\mathbf{F}^{n+1/2}. \tag{7.10}$$

Let $\mathbf{Q} = \left(\mathbf{I} - \frac{\Delta t}{2}\mathbf{A}\right)^{-1}\left(\mathbf{I} + \frac{\Delta t}{2}\mathbf{A}\right)$ be the amplification matrix. Since $\mathbf{A}$ is negative definite, the eigenvalues μ_j of $\mathbf{A}$ are real and non-positive. The eigenvalues of $\mathbf{Q}$ are given by:

$$\lambda_j(\mathbf{Q}) = \frac{1 + \frac{\Delta t}{2}\mu_j}{1 - \frac{\Delta t}{2}\mu_j}. \tag{7.11}$$

Since $\mu_j \leq 0$, it follows that $|\lambda_j(\mathbf{Q})| \leq 1$. Thus, $\|\mathbf{Q}\|_2 \leq 1$. Taking the norm of the update equation:

$$\|\mathbf{C}^{n+1}\|_2 \leq \|\mathbf{Q}\|_2\|\mathbf{C}^n\|_2 + \Delta t\left\|\left(\mathbf{I} - \frac{\Delta t}{2}\mathbf{A}\right)^{-1}\right\|_2\|\mathbf{F}^{n+1/2}\|_2 \tag{7.12}$$

$$\leq \|\mathbf{C}^n\|_2 + \Delta t\|\mathbf{F}^{n+1/2}\|_2, \tag{7.13}$$

where we used the fact that $\|(\mathbf{I} - \frac{\Delta t}{2}\mathbf{A})^{-1}\|_2 \leq 1$ because the eigenvalues of the inverse are $(1 - \frac{\Delta t}{2}\mu_j)^{-1} \leq 1$. This proves (7.9). □

Main Convergence Theorem: We now combine the spatial projection error and the temporal discretization error to establish the total convergence rate of the method. Let $u(r, \theta, t)$ be the exact solution and $u_N^k(r, \theta)$ be the fully discrete numerical solution at time $t_k = k\Delta t$.

Theorem 7.2 (Total Error Estimate). *Let $u \in C^3([0,T]; H^s_w(\Omega))$ be the exact solution of the heat equation* (2.1)*. Let u^k_N be the numerical solution obtained via the Bessel Collocation Method with N radial modes and time step Δt. Then, there exists a constant $C > 0$ independent of N and Δt such that:*

$$\max_{0 \le k \le T/\Delta t} \|u(\cdot, t_k) - u^k_N\|_w \le C\left(N^{-s} + \Delta t^2\right). \tag{7.14}$$

If u is analytic in space, the spatial term N^{-s} is replaced by $e^{-\sigma N}$.

Proof. Let $e^k = u(\cdot, t_k) - u^k_N$ be the total error at time step k. We decompose the error using the triangle inequality:

$$\|e^k\|_w \le \|u(\cdot, t_k) - \Pi_N u(\cdot, t_k)\|_w + \|\Pi_N u(\cdot, t_k) - u^k_N\|_w. \tag{7.15}$$

Denote $\eta^k = u(\cdot, t_k) - \Pi_N u(\cdot, t_k)$ as the projection error and $\xi^k = \Pi_N u(\cdot, t_k) - u^k_N$ as the discrete evolution error. From Lemma 7.1, we have $\|\eta^k\|_w \le C_1 N^{-s}$.

To bound ξ^k, we derive the error equation. The exact solution projected onto $\mathcal{P}_N$ satisfies:

$$\frac{\Pi_N u^{k+1} - \Pi_N u^k}{\Delta t} = \mathbf{A}_N \frac{\Pi_N u^{k+1} + \Pi_N u^k}{2} + \Pi_N f^{k+1/2} + \tau^k, \tag{7.16}$$

where $\mathbf{A}_N$ is the discrete operator on $\mathcal{P}_N$ and τ^k is the local truncation error of the Crank-Nicolson scheme, satisfying $\|\tau^k\|_w \le C_2 \Delta t^2 \|u_{ttt}\|_w$. The numerical solution satisfies the same equation without τ^k. Subtracting the two equations yields:

$$\frac{\xi^{k+1} - \xi^k}{\Delta t} = \mathbf{A}_N \frac{\xi^{k+1} + \xi^k}{2} - \tau^k. \tag{7.17}$$

Rearranging and taking norms, utilizing the stability result from Theorem 7.1:

$$\|\xi^{k+1}\|_w \le \|\xi^k\|_w + \Delta t \|\tau^k\|_w. \tag{7.18}$$

Recursively applying this inequality from $k = 0$ to n (where $t_n \le T$):

$$\|\xi^n\|_w \le \|\xi^0\|_w + \sum_{j=0}^{n-1} \Delta t \|\tau^j\|_w \le \|\xi^0\|_w + T C_2 \Delta t^2. \tag{7.19}$$

Assuming the initial condition is projected accurately, $\|\xi^0\|_w \le C_1 N^{-s}$. Combining the bounds for η and ξ:

$$\|e^n\|_w \le C_1 N^{-s} + C_1 N^{-s} + T C_2 \Delta t^2 \le C(N^{-s} + \Delta t^2). \tag{7.20}$$

This completes the proof. □

Discussion of Numerical Results: The theoretical bounds derived in Theorem 7.2 align perfectly with the numerical data presented in Table 2 of Section 3.

- **Spatial Convergence:** The error reduction from 10^{-2} to 10^{-16} as N_r increases from 4 to 24 indicates exponential convergence ($e^{-\sigma N}$), confirming that the test problem possesses analytic regularity, satisfying the stronger condition of Lemma 7.1.

- **Temporal Convergence:** The use of the Crank-Nicolson scheme ensures second-order accuracy in time ($O(\Delta t^2)$). In the numerical experiments, Δt was chosen sufficiently small (10^{-4}) such that the spatial error dominated, allowing the spectral accuracy of the BCM to be observed clearly.
- **Stability:** The absence of oscillatory blow-up in the numerical results, even for larger N_r, validates the unconditional stability proved in Theorem 7.1.

This analysis confirms that the Bessel Collocation Method is not only computationally efficient but also theoretically robust for solving heat conduction problems in circular domains.

8. Conclusion

This work establishes a comprehensive framework for solving the heat conduction equation in cylindrical domains with time-dependent polynomial and harmonic boundary conditions. The analytical solution, constructed via superposition and Fourier-Bessel series, is proven convergent in L_2 norm and asymptotically stable. The Bessel Collocation Method provides an efficient numerical implementation with spectral spatial accuracy and second-order temporal accuracy.

Key contributions include: (1) transformation of non-homogeneous boundary problems via reference functions; (2) rigorous convergence proofs using orthogonality of Bessel eigenfunctions; (3) demonstration of boundary synchronization in long-time behavior; (4) development of a spectrally accurate numerical method with verified error estimates.

The methodology extends to other Laplacian-based problems including wave propagation, diffusion in porous media, and stress analysis. Future work will address multi-layered cylinders and nonlinear boundary conditions.

Conflicts of Interest: The authors declare that there are no conflicts of interest regarding the publication of this paper.

References

[1] C. Canuto, M.Y. Hussaini, A. Quarteroni, T.A. Zang, Spectral Methods: Fundamentals in Single Domains, Springer, Berlin, 2006. https://doi.org/10.1007/978-3-540-30726-6.

[2] J. Shen, T. Tang, L. Wang, Spectral Methods: Algorithms, Analysis and Applications, Springer, Berlin, 2011. https://doi.org/10.1007/978-3-540-71041-7.

[3] J.P. Boyd, Chebyshev and Fourier Spectral Methods, Dover Publications, Mineola, 2001.

[4] L.N. Trefethen, Spectral Methods in MATLAB, SIAM, 2000. https://doi.org/10.1137/1.9780898719598.

[5] A.N. Tikhonov, A.A. Samarskii, Equations of Mathematical Physics, Nauka, 1972.

[6] O.A. Ladyzhenskaya, The Boundary Value Problems of Mathematical Physics, Springer, New York, 1985. https://doi.org/10.1007/978-1-4757-4317-3.

[7] S.L. Sobolev, Equations of Mathematical Physics, Nauka, 2009.

[8] K.Y. Kung, M.F. Gong, H.M. Srivastava, S.D. Lin, Analytic Transient Solutions of a Cylindrical Heat Equation, Filomat 35 (2021), 2617–2628. https://doi.org/10.2298/FIL2108617K.

[9] T.W. Tu, S.Y. Lee, Analytical Solution of Heat Conduction for Hollow Cylinders with Time-Dependent Boundary Condition and Time-Dependent Heat Transfer Coefficient, J. Appl. Math. 2015 (2015), 203404. https://doi.org/10.1155/2015/203404.

[10] Z.D. Abbasov, A Mixed Boundary Value Problem for the n-Dimensional Wave Equation, Sci. Res. Int. Online Sci. J. 3 (2023), 23–28.

[11] K.V. Zhukovsky, H.M. Srivastava, Analytical Solutions for Heat Diffusion beyond Fourier Law, Appl. Math. Comput. 293 (2017), 423–437. https://doi.org/10.1016/j.amc.2016.08.038.

[12] Z.D. Abbasov, Mathematical Physics Equations, Elm va T'ahsil, Baku, 2018.

[13] W.M. Abd-Elhameed, Y.H. Youssri, Sixth-Kind Chebyshev Spectral Approach for Solving Fractional Differential Equations, Int. J. Nonlinear Sci. Numer. Simul. 20 (2019), 187–201. https://doi.org/10.1515/ijnsns-2018-0118.

[14] Y.H. Youssri, Orthonormal Ultraspherical Operational Matrix Algorithm for Fractal–Fractional Riccati Equation with Generalized Caputo Derivative, Fractal Fract. 5 (2021), 100. https://doi.org/10.3390/fractalfract5030100.

[15] A.G. Atta, Y.H. Youssri, Advanced Shifted First-Kind Chebyshev Collocation Approach for Solving the Nonlinear Time-Fractional Partial Integro-Differential Equation with a Weakly Singular Kernel, Comput. Appl. Math. 41 (2022), 381. https://doi.org/10.1007/s40314-022-02096-7.

[16] R.M. Hafez, Y.H. Youssri, Shifted Gegenbauer-Gauss Collocation Method for Solving Fractional Neutral Functional-Differential Equations with Proportional Delays, Kragujevac J. Math. 46 (2022), 981–996. https://doi.org/10.46793/KgJMat2206.981H.

[17] Y.H. Youssri, R.M. Hafez, A.G. Atta, An Innovative Pseudo-Spectral Galerkin Algorithm for the Time-Fractional Tricomi-Type Equation, Phys. Scr. 99 (2024), 105238. https://doi.org/10.1088/1402-4896/ad74ad.

[18] M. Abdelhakem, D. Abdelhamied, M. El-Kady, Y.H. Youssri, Two Modified Shifted Chebyshev–Galerkin Operational Matrix Methods for Even-Order Partial Boundary Value Problems, Bound. Value Probl. 2025 (2025), 34. https://doi.org/10.1186/s13661-025-02021-x.

[19] Y.H. Youssri, M.A. Zaky, R.M. Hafez, Romanovski-Jacobi Spectral Schemes for High-Order Differential Equations, Appl. Numer. Math. 198 (2024), 148–159. https://doi.org/10.1016/j.apnum.2023.12.015.

[20] Y. Youssri, A. Atta, Explicit Chebyshev Collocation Method for Multi-Order Fractional Nonlinear Boundary Value Problems in Mathematical Chemistry, Iran. J. Math. Chem. 16 (2025), 257–273. https://doi.org/10.22052/IJMC.2025.256602.1997.